

## Vortices of polarization in BaTiO<sub>3</sub> core-shell nanoceramics: Calculations based on *ab initio* derived Hamiltonian versus Landau theory

M. Anoufa,<sup>1</sup> J. M. Kiat,<sup>1,2</sup> I. Kornev,<sup>1</sup> and C. Bogicevic<sup>1</sup>

<sup>1</sup>Laboratoire Structures, Propriétés et Modélisation des Solides, Ecole Centrale Paris, CNRS-UMR8580, Grande Voie des Vignes, 92295 Châtenay-Malabry Cedex, France

<sup>2</sup>Laboratoire Léon Brillouin, CE Saclay CNRS-UMR12, 91991 Gif-sur-Yvette Cedex, France

(Received 24 June 2013; revised manuscript received 4 September 2013; published 18 October 2013)

In this paper, we want to emphasize the fact that many experimental properties of ceramics can be explained by the existence of a core-shell structure of the grains, particularly at small sizes. In this framework, we have studied BaTiO<sub>3</sub> (BT) ceramics constituted of core-shell nanoparticles, nanowires, or nanoplates by using *ab initio* derived effective Hamiltonian calculations whose application range is for large values of shell thickness and low values of shell permittivity. Many differences and new features compared to the situation of nanodots are induced by the core-shell structure. For instance, phase sequences are different; there is also a coexistence of vortices found by Naumov, Bellaïche, and Fu [I. I. Naumov, L. Bellaïche, and H. Fu, *Nature (London)* **432**, 737 (2004)] in the case of isolated dots with a homogeneous polarization, a transition from cubic paraelectric phase towards nonpolar rhombohedral phase, anomalies in dielectric permittivity associated with the onset of toroidal moments, etc. Afterwards, we compare these results with those obtained by the Landau theory of core-shell ceramics we have recently published. However, the *ab initio* calculations fail to capture the physics at small shell thickness and/or high shell permittivity, whereas the Landau theory fails to predict the peculiar properties of the phases in which vortices exist. Therefore, in a tentative way to build a global theory, we have constructed a Landau potential using both the polarization and the toroidal moment as competing order parameters, which allows us to propose a phase diagram, whatever the thickness and permittivity of the shell are.

DOI: [10.1103/PhysRevB.88.144106](https://doi.org/10.1103/PhysRevB.88.144106)

PACS number(s): 64.60.-i, 77.80.B-, 61.46.-w

### I. INTRODUCTION

The question of reduction of sizes in ferroelectric materials is the subject of many fundamental and applied researches, both of them motivated by an increasing number of industrial applications. This is an important problem, for instance, in the case of multilayer ceramic capacitors and actuators. Indeed, decreasing the thickness of such devices for their integration in microelectronic systems below micrometer sizes requires controlling the structure and properties of nanosized particles, both of them are known to drastically change at the smallest sizes. Indeed, a huge number of experimental studies have shown that the reduction of size in ceramic grains is accompanied by a drastic diminishing of the dielectric permittivity, a shift of the ferroelectric to paraelectric transition, and eventually the disappearance of macroscopic ferroelectricity. However, many reports of ferroelectricity in BaTiO<sub>3</sub> (BT) at small sizes published in the 1990s<sup>1</sup> reported a critical size of  $\approx 100$  nm, a value which continuously decreased as time passed, to reach nano or subnanometer values in the most recent papers. In “simple” ferroelectrics such as BT or PbTiO<sub>3</sub> (PT), the situation is now well documented: it is clear from both experiments and *ab initio* calculations that the ferroelectric ground state should remain stable below at least 10 nm or less. In BT (and probably PT), the size and temperature dependencies of permittivity in ceramics down to 10 nm can be quantitatively explained by a core-shell structure of the grains,<sup>1,2</sup> in which the core behaves like the bulk material but is subject to a pure size effect, whereas the shell is the part of the particle close to the surface in which extrinsic effects occur, with typical thickness of  $\approx 1$  nm and a permittivity much lower than that of the core (typically around  $\epsilon_r = 70$ ).

We have extended this picture to lead-based relaxor and morphotropic compounds<sup>3-6</sup> and to quantum paraelectric strontium titanate, SrTiO<sub>3</sub> (STO).<sup>7</sup> The precise microscopic structure of the shell (or dead layer) is in most of the cases unclear as it strongly depends on the synthesis route, the sintering process, the presence of impurity ions or vacancies, etc., but is clearly connected to the local structure and chemical composition of the grain boundary. In many cases, during synthesis, core-shell structures are more or less unavoidable (we call this situation “natural” core shell in the rest of the text) but it can also be induced on purpose, e.g., (Refs. 8 and 9) to tailor physical properties (“artificial” core-shell). This can be done, e.g., by doping with specific ions, which diffuse weakly inside the particles and remain mainly close to the surface of the grains, or by coating the grains by another compound with much lower permittivity, typically, silica (SiO<sub>2</sub>) or alumina (Al<sub>2</sub>O<sub>3</sub>) to increase densification and get a gigantic Maxwell Wagner permittivity. In this latter case, a core-double shell is sometimes observed, i.e., natural plus artificial core-shell structure.

From the standpoint of modeling, there are also many attempts to explain and clarify the experimental situation. Several types of approaches have been used, either analytically, or in the framework of effective media approaches (EMA), brick-layer-type models, or Landau theory. These methods have tried to take into account the complex situation in ceramics, eventually at nanometer sizes, and many of them separate the microscopic structure of the grains as a “core,” which behaves as bulk material submitted to a “pure” size effect, and a “shell” in which all nonintrinsic effects such as defects of all kinds including vacancies, dead layers, internal strains, etc., occur. For instance, Emelyanov *et al.*<sup>10</sup> have partially explained

dielectric properties of ferroelectric ceramics by the presence of fixed-thickness dielectric dead layer at grain boundaries. Very recently, we have shown<sup>11</sup> by using a combination of the effective medium approximation and Landau theory that core-shell structures should be considered, indeed, as the main parameter to explain the dielectric properties of barium titanate as well as its ferroelectric transitions at nanometer sizes. However, these types of methods cannot predict the microscopic organization of the polarization at a very local state in ceramics.

In recent years, effective Hamiltonians and *ab initio* calculations have received a huge success. It is true that these methods have allowed a deep understanding of ferroelectricity at nanometer sizes, and many new effects, such as the existence of vortices of polarization in nanodots have been predicted<sup>12-14</sup> and subsequently experimentally verified.

However, up to now, these methods have mostly dealt with the case of “independent” or “elastic free” nanoparticles, which are relevant for technological applications such as memories, but are not intended for the case of nanostructured ceramics in which the nanograins strongly interact with each other elastically and electrically and in which a core-shell structure is observed. In analogy with the situation of nanodots modeled by *ab initio* methods, one may wonder whether a nanoceramic could adopt new forms of polar organization (such as vortices, for instance). Indeed, to the best of our knowledge, no attempts have been made to resolve this issue in the framework of first-principles calculation.

Therefore the aim of this paper is to give results in core-shell nanoceramics of BaTiO<sub>3</sub> system obtained from an *ab initio* derived effective Hamiltonian method. We give results for ceramics built of core-shell nanodots, and describe briefly the case of ceramics built on core-shell nanowires; the case of nanoplanes is also shortly addressed as it is physically relevant in the field of thin films and the problem of dead layers. Afterwards, we address the comparison of these results with the situation of isolated nanodots as calculated in Refs. 12,13, and 14, then compare with the situation of nanoceramics in the framework of the Landau theory from our previous work. Finally, in order to catch other physical insights, which are unreachable via *ab initio* derived effective Hamiltonian calculations, we propose a Landau-based formalism, using a toroidal moment as the order parameter; in particular, a phase diagram is predicted and discussed.

## II. METHODOLOGY

We decided to model a ceramic in which the grains are made of core-shell particles, i.e., nanodots, which are periodically repeated in space by using infinitely periodic boundaries. This is very different from previous works which considered isolated (pure core) nanodots and the differences and the consequences of these hypotheses will be discussed in Sec. IV A. We used BT as the core material, and a dielectric shell of thickness  $e$  and low permittivity  $\epsilon_r$ : its chemical composition could be either BT with defects, vacancies, etc., corresponding to a “natural” shell or it could be made of artificial coating. In fact, we observed that the results of calculations depend strongly on  $e$  and  $\epsilon_r$  but weakly on the exact chemical composition of the shell. We have considered an infinitely periodic structure

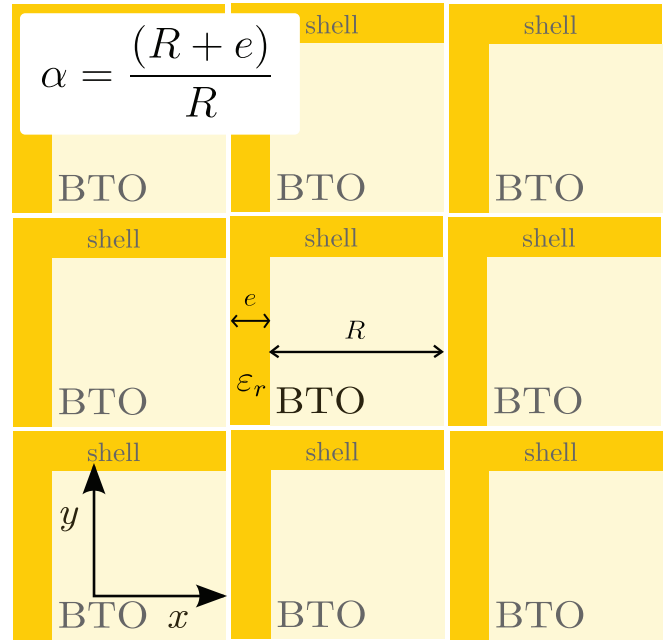


FIG. 1. (Color online) Periodic core-shell unit pattern of the nanodots as modeled in this work. In the case of nanodots, the distance  $R$  is along the three  $x$ ,  $y$ , and  $z$  directions, in the case of nanowires,  $R$  is along  $x$  and  $y$  directions and infinite along  $z$  direction, and in the case of nanoplanes,  $R$  is along  $z$  direction, and is infinite along the two other directions.

as shown of Fig. 1 in which a “unit” cell formed of a core of length  $R$  with three perpendicular boundary shells with thickness  $e$ , periodically repeats along the  $x$ ,  $y$ , and  $z$  directions;  $\alpha = (R + e)/R$  is thus the thickness ratio, equal to 1 if no shell is present, thus the situation of an infinite (i.e., bulk) single crystal is recovered. The case of core-shell nanowire ceramics can be obtained by suppressing the shell perpendicular to one direction, e.g., the  $z$  direction, and the case of nanoplane ceramics by suppressing the shell perpendicular to two directions, e.g., the  $y$  and  $z$  directions.

The calculation is using the effective Hamiltonian coupled with Monte Carlo simulations developed by Zhong, Vanderbilt, and Rabe,<sup>15</sup> which targets in particular ferroelectric perovskites. In this approach, local modes  $u_i$  ( $i$  is the cell index) describe the ferroelectric instability in individual 5-atom ABO<sub>3</sub> cells;  $u_i$  are associated with local electrical dipoles  $P_i$  via  $P_i = Z^* u_i$  (where  $Z^*$  is the effective charge of the local mode). The total energy is written as

$$E_{\text{tot}} = E_{\text{self}}(u) + E_{\text{dpl}}(u) + E_{\text{short}}(u) + E_{\text{elas}}(\eta) + E_{\text{int}}(u, \eta),$$

where  $\eta$  is the strain.

This development is well known and will not be explained here: let us just recall that the first term is the energy corresponding to the local modes, the second one to the long-range dipole-dipole interaction, the third one to the short-range interaction, the fourth one to the elastic interaction, and the fifth one to the dipole-elastic interaction.

Compared to the original method, we have made new developments in order to be able to study core-shell nanoparticles. We have therefore taken into account the presence of two different phases: (1) the core phase, which is modeled with

TABLE I. Effective Hamiltonian parameters used for ceramics built on particles with a core of BT and a shell of SiO<sub>2</sub>.

Effective Hamiltonian parameters	BaTiO <sub>3</sub> core	SiO <sub>2</sub> shell
Lattice constant $a$	7.371	7.371
$Z_{\text{eff}}$	9.6646	9.6646
$\varepsilon_{\infty}$	5.21	5.21
$\kappa_2$	0.051758	0.08
$\alpha$	0.2808	0.1
$\gamma$	-0.41281	-0.1228
$j_1$	-0.0120107708	-0.0120107708
$j_2$	0.0222156256	0.0222156256
$j_3$	0.0042062141	0.0042062141
$j_4$	-0.0023677794	-0.0023677794
$j_5$	0.003536007	0.003536007
$j_6$	0.0007541296	0.0007541296
$j_7$	0.000377065	0.000377065
$B_{11}$	4.776	1.195
$B_{12}$	1.610	0.402
$B_{1xx}$	-1.973	-0.0273
$B_{1yy}$	-0.041	-0.041
$B_{4yz}$	-0.059	-0.059

the well-known Hamiltonian parameters, and (2) the shell phase, which should have the physical characteristics of a linear dielectric.

Since the Hamiltonian code developed by Vanderbilt *et al.* is adapted to the perovskite structure, the shell phase should be modeled also as a perovskite ABO<sub>3</sub>, which is the case of many experimental situations, and therefore we have empirically adapted the Hamiltonian in order to fit the chosen material with a low value of permittivity  $\varepsilon_r$ . We have considered in some calculation the case of artificial shell made of SiO<sub>2</sub> (with permittivity ranging from  $\varepsilon_r = 3$ ) and calculated a “pseudoperovskite” with Hamiltonian parameters that mimic the dielectric and elastic behavior of real silica. In particular, short-range interactions have been drastically reduced in this pseudoperovskite phase. Table I shows Hamiltonian parameters that have been used for the BaTiO<sub>3</sub> core-phase and pseudosilica shell phase.

Since the dielectric shell is modeled by a perovskite, its thickness in the elementary cell (see Fig. 1) cannot be reduced to less than one lattice parameter (about 4 Å). Therefore in practice, in order to diminish the “radius” ratio  $\alpha$ , we need to change essentially the BaTiO<sub>3</sub> core size  $R$ . We have modeled the core-shell system for sizes (expressed in  $N \times N \times N$  lattices) ranging from  $N = 6$  to 28 (i.e., a maximum size for BT of  $\approx 12$  nm), which correspond to  $\alpha$  ratio from 1.16 to 1.035, respectively, that is, 16% and 3.5% of thickness  $\alpha$  ratio of the shell/core. Trying to go to lower values of  $\alpha$  should involve using larger cells, which is not possible due to the computing time limitation. To get insight into the situation at lower thickness of the shell, or for other materials, we have increased the value of  $\varepsilon_r$ . However, strong increases of this value will at some point induce ferroelectricity in the shell, which should give rise to a strongly nonlinear (versus temperature and electric field) permittivity; this should be avoided in order to accurately describe a linear dielectric shell.

We have studied the response of such core-shell nanoceramic at quasinull field and at high field. At quasinull fields, we have observed that up to  $\varepsilon_r \approx 90$  no peak in the temperature dependence of permittivity (which should have indicated a ferroelectric phase) was observed; at high electric fields a value of  $\varepsilon_r$  not higher than  $\approx 20$  should be used for the same reasons. However, in this paper, we will show only results obtained in the low-field limit and therefore values of  $\varepsilon_r$  up to 90 could be safely used. Results at high field will eventually be published elsewhere. As usual, the total energy is used in Monte Carlo simulations to obtain finite-temperature properties and to get the most pertinent equilibrium state. The simulations have been performed from “high” temperature ( $T = 800$  K) down to  $T = 0$  K.

### III. RESULTS

#### A. Case of nanoceramics constituted of core-shell nanodots

We have calculated the Cartesian components  $u_x$ ,  $u_y$ ,  $u_z$  of the local mode—which is directly proportional to the polarization—in nanodots with  $x$ ,  $y$ , and  $z$  axes being along the pseudocubic 100, 010, and 001 directions. Figure 2 shows a comparison of results for bulk BT ( $\alpha = 1$ ) and for the core-shell ceramic. In the case of the bulk BT, we get of course the well-known cubic (C), tetragonal (T), orthorhombic (O) and rhombohedral (R) phases. However, in the case of the ceramic, even for the smallest values of shell thickness, which can be calculated, i.e.,  $\alpha = 1.035$ , we have observed only a very weak residual polarization, less than 1/10 of bulk BT, which means a disappearance of any macroscopic ferroelectricity; above 200 K (see enlargement in insert of Fig. 2), this residual value completely disappears.

However, at microscopic scale, there is a well-defined organization of the local polarization, very similar to what found by Naumov *et al.*<sup>12</sup> in the case of isolated dots (i.e., in open-circuit condition). Indeed, the local modes rotate around

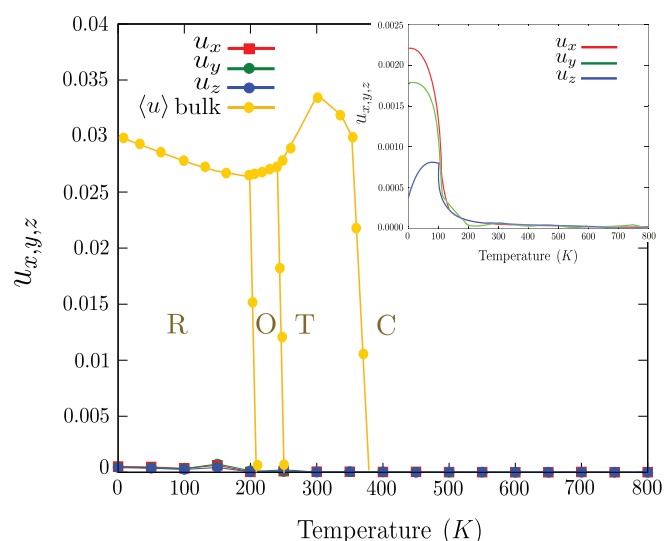


FIG. 2. (Color online) Local modes calculated for a single crystal of BT and in the insert, calculation for a ceramic constituted of core-shell nanodots: in this latter case, only residual polarization is observed below 200 K.

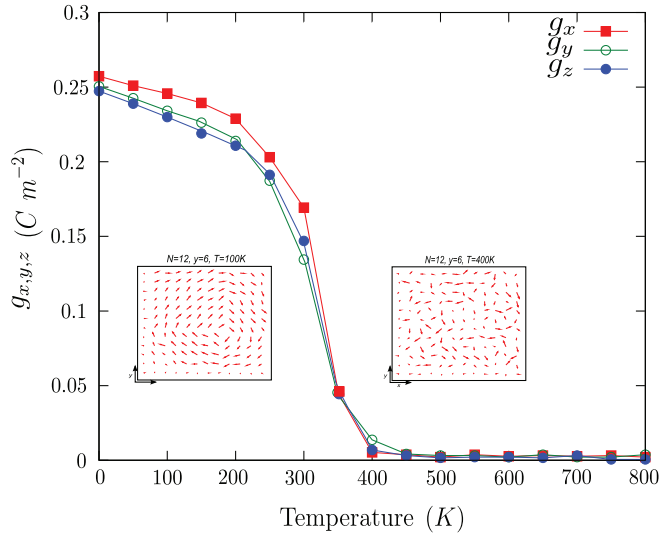


FIG. 3. (Color online) Temperature dependence of the components of the toroidal moment, in the case of a ceramic constituted of core-shell nanodots. (Insert) Projection of the local polarization along the  $x'y$  plane showing appearance of vortices at low temperatures.

the [111] diagonal direction of the cube and form a vortex. A projection of this configuration into the plane perpendicular to one of the cubic simple directions (left insert of Fig. 3) shows that this 3D configuration can be considered as a vector composition of rotations along the 3 axis.

That is why Naumov *et al.* demonstrated that such microscopic organization of polarization can be quantified by using the toroidal moment  $G$ :

$$G = \frac{1}{2M} \sum_i \mathbf{R}_i \cdot (\mathbf{p}_i - \langle \mathbf{p} \rangle), \quad (1)$$

where  $R_i$  correspond to the  $i$  coordinate of the punctual dipole  $p_i$  with  $\langle p \rangle$  the mean punctual dipole and  $M = N^3$ , where  $N$  is the size of the supercell. This toroidal moment has been proposed as a new order parameter for the microscopic situation of nanodots. However, we can observe from its dimensional analysis that this quantity is not normalized: indeed, it can be shown that the toroidal moment as expressed above increases with the size of the cell by an  $N$  factor. To show that, we can consider a simplified situation where we replace the  $N \times N \times N$  cubic cell by a cylinder with a diameter  $D = Na$  (where  $a$  is the unit cell length) and height  $Na$ . In a situation where all dipoles get the same  $p_{\perp} = |\mathbf{p}_{\perp}|$  norm and rotate around the  $z$  axis of the cylinder, the toroidal moment is along  $z$  ( $G_x = G_y = 0$ ); indeed, from the above definition and since by symmetry  $\langle p \rangle = 0$ ,

$$G = \frac{1}{2M} \sum_i \mathbf{R}_i \cdot \mathbf{p}_{\perp}.$$

In the cylindrical coordinate system, the  $\mathbf{R}_i$  vector can be decomposed into a radial and a  $z$  component:

$$\mathbf{R}_i = R_{ir} \mathbf{u}_r + R_{iz} \mathbf{u}_z.$$

We can therefore write

$$\mathbf{G} = \frac{1}{2M} \left( \sum_i \mathbf{R}_{ir} \cdot \mathbf{p}_{\perp} + \sum_i \mathbf{R}_{iz} \cdot \mathbf{p}_{\perp} \right),$$

where the second sum is null due to symmetry considerations. The toroidal moment is therefore aligned with the  $z$  axis with

$$G_z = \frac{1}{2M} N \sum_{r=0}^{\frac{D}{2}} r a p_{\perp} (2\pi r) = \frac{1}{4M} N a p_{\perp} \pi \sum_{d=0}^N d^2.$$

In a cylinder,  $M = \pi \left(\frac{N}{2}\right)^2 N = \frac{\pi}{4} N^3$ , consequently,

$$G_z = \frac{a \cdot p_{\perp}}{N^2} \sum_{d=0}^N d^2.$$

Using

$$\sum_{d=0}^N d^2 = \frac{1}{6} N(N+1)(2N+1),$$

we can see that for  $N \gg 1$ ,

$$\sum_{d=0}^N d^2 \approx \frac{1}{3} N^3,$$

and we can therefore write

$$G_z \approx \frac{1}{3} a p_{\perp} N,$$

which shows that  $G$  is linearly dependent on the  $N$  size. Therefore we have used for our study instead of  $G$  the vector quantity  $\mathbf{g}$  as order parameter defined as follows:

$$g_{\alpha} = \frac{p_{\perp \alpha}}{a^3} \approx \left( \frac{G_{\alpha}}{N} \right) \frac{3}{a^4}$$

(with  $\alpha = x, y, z$ ); notice that  $\mathbf{g}$  has the same dimensionality as the polarization since it represents the volume average of the norm of cell polarization induced by the presence of a toroidal moment. The temperature evolution is shown in Fig. 3: the three components  $g_i$  are zero above  $T \approx 400$  K (which corresponds to the Curie temperature of bulk  $\text{BaTiO}_3$ ), whereas below this temperature, an order-parameter-like behavior is observed.

We have also calculated the different components of the normal and shear strains (see Fig. 4). The main components of the strain are the normal components, which are by a factor 30 greater than the shear components. Whereas the sole consideration of polarization should have indicated a (C) cubic phase, all strain curves clearly indicate at low temperatures the existence of a rhombohedral distortion (the three components are approximately equal for both normal and shear strain), whose magnitude is at 0 K about four times smaller than in bulk rhombohedral BT. This result is a natural consequence of the fact that the local modes rotate in the form of a vortex along the [111] direction. In other words, the toroidal moment induces an elastic deformation, which is rhombohedral but not ferroelectric; we call this phase C' hereafter in the text, the prime is to indicate that it is an elastic/structural distortion of the standard (C) cubic phase of BT, and that it is different from the (R) phase of bulk BT, which is ferroelectric. Above

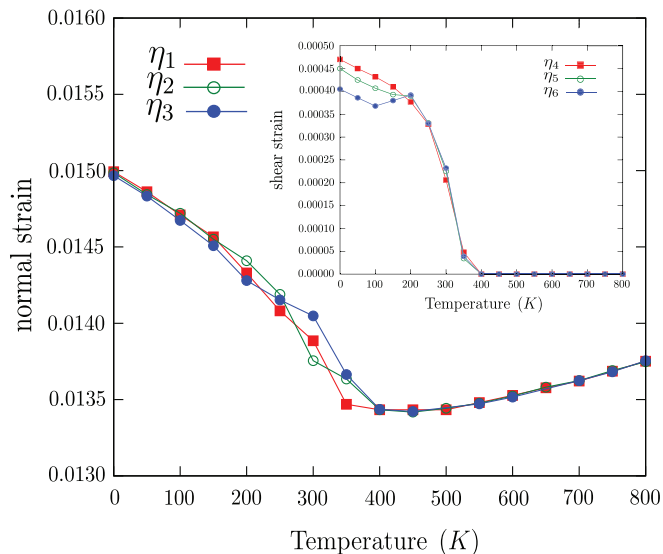


FIG. 4. (Color online) Temperature dependence of the components of the normal strain and, in insert, of the shear strain, in the case of a ceramic constituted of core-shell nanodots. In the latter case, the values are very weak.

$T \approx 400$  K, the shear distortion vanishes because the toroidal moment also does so, the remaining normal strain is just the strain associated to normal thermal dilatation: the phase becomes the standard (C) cubic phase of BT.

These results indicate that the microscopic polar organization in BT nanoceramics for  $T < 400$  K is very different from the typical polar disorder expected in a classical paraelectric. Moreover, the presence of a shear strain in the nanoceramics at  $T < 400$  K is an intrinsic phenomenon, which superimposes to usual internal shear stress effects almost always observed in disordered nanoceramics. Therefore our results show that the strain associated to the existence of a toroidal moment cannot be released by any adequate thermal treatments. This new (C') rhombohedral phase is a nonpolar phase as no macroscopic polarization exists, and is to be associated to the onset of the new order parameter associated to the existence of a toroidal moment.

We have also calculated the dielectric permittivity (at zero field) and got a surprising result (see Fig. 5, two plain lines with dots). Indeed, we observed two weak but well pronounced peaks, the first one is at  $\approx 180$  K, the second one is at  $\approx 320$  K. The first peak is to be associated with the existence of the residual polarization below 200 K, as observed in Fig. 2; the second one is more surprising as it is not related to any polarization but to the onset of cooling of the vortices of polarization. This origin will be clearly demonstrated in Sec. IV D in which we calculate the permittivity associated to the onset of toroidal moment (see Fig. 5, dotted line).

Up to now, we have studied the case of nanodots with a shell structure sufficiently thick to induce a depolarizing field that is strong enough to cancel the polarization. The case of shells with weaker thickness is also interesting to examine as it should indicate how one passes from the situation of core-shell nanodots, with no macroscopic ferroelectric polarization, to the case of infinite bulk ferroelectric single crystal. However, as we have indicated in Sec. II, we cannot go below the

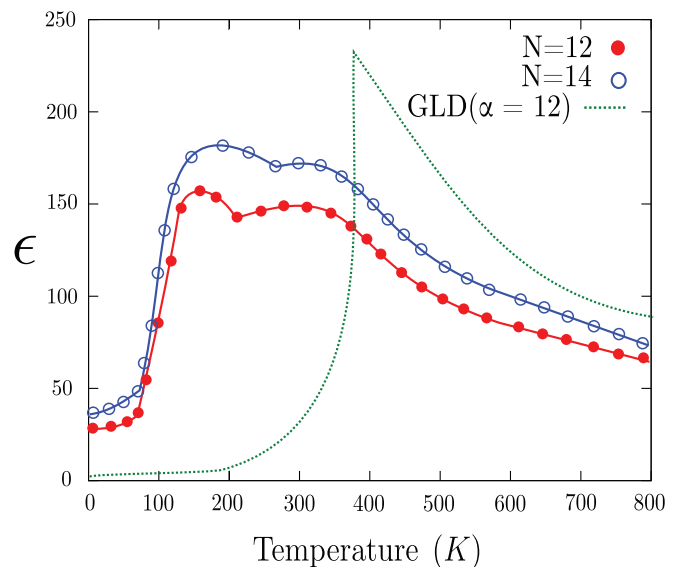


FIG. 5. (Color online) Temperature dependence of the dielectric permittivity in the case of a ceramic constituted of core-shell nanodots, for two values of the size system  $N \times N \times N$ . One peak (at low temperature) is associated with the onset of the residual polarization, the second one (at high temperature) to the onset of the toroidal moment. Also, dotted line (see text below in Sec. IV D), we show the temperature dependence of dielectric permittivity calculated by the Landau theory using  $g$  and  $P$  as order parameters for a core-shell nanodots ceramic, in the case of high value of  $\alpha = 1.02$  for which no ferroelectric transition occurs: a clear anomaly is observed, associated to the onset of the toroidal moment.

shell with  $\alpha = 1.035$ . Instead, another way to diminish the depolarizing field responsible for the core-shell behavior is to increase the value of  $\epsilon_r$ , which we can reliably do up to a value of  $\approx 90$ , as explained in Sec. II. We did not explore all the details of this situation but globally we observe the onset of a macroscopic polarization and a diminishing of the components of the toroidal moment with situations in which both polarization and toroidal moment coexist inside a temperature range (see Fig. 6).

### B. Case of nanoceramics constituted of core-shell nanowires

In our previous work,<sup>2</sup> we have shown that properties of nanostructured ceramics can be greatly enhanced, in particular for energy-harvesting applications, if instead of core-shell dots (i.e., spherical), the ceramic is built from nanodisks or

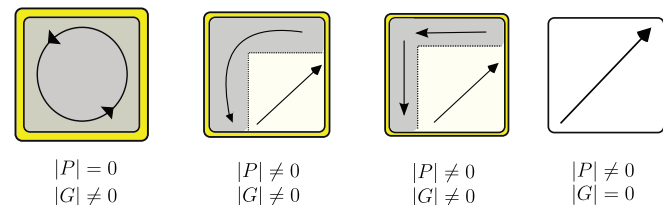


FIG. 6. (Color online) Schematic representation of the toroidal moment and of the macroscopic polarization for a decreasing shell thickness or increasing shell permittivity: one passes from a situation with a pure vortex configuration to a mixed situation in which ferroelectric domains progressively grow against the vortices.

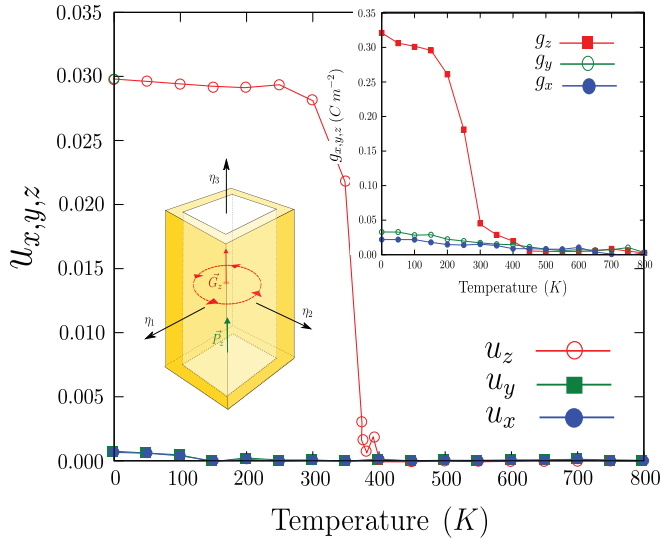


FIG. 7. (Color online) Temperature dependence of the components of local modes and in the insert of the toroidal moment in the case of a ceramic constituted of core-shell nanowires. In the insert, we also show the schematic representation of the nanowire with coexistence of vortices and macroscopic polarization: only a  $P_z$  macroscopic component is observed and in the perpendicular plane the local polarization adopts a vortex pattern, i.e., a  $g_z$  component is only observed.

nanowires with a core-shell structure. Although such types of ceramic are not very easily synthesized as all disks or wires should be aligned in the same direction, experimental efforts are done to achieve such nanostructured ceramics. The calculation shown above can easily be performed in the case of infinite core-shell nanowires, assuming an infinite  $z$  direction and a coating only along  $x = 1$  and  $y = 1$  planes. The results (see Fig. 7) show that the  $x$  and  $y$  components of polarization are approximately zero, whatever the temperature is, like in the case of core-shell nanodots, but a strong  $z$  component is observed, with a value close to that of the bulk material, at temperatures below  $\approx 400$  K. This result can be intuitively understood by considering the fact that along the  $z$  direction no depolarizing field exists.

Although  $x$  and  $y$  components of polarization are approximately zero, they display nonzero toroidal moment along the  $z$  direction (two insert of Fig. 7), below the same temperature  $\approx 400$  K with a magnitude comparable to the case of core-shell nanodots. This temperature therefore corresponds to the onset of a ferroelectric tetragonal phase in which axial polarization coexists with planar vortices.

In this phase, the origin of the tetragonal distortion is thus twofold: a contribution due to the coupling of polarization with lattice, like in bulk BT, plus a contribution due to toroidal moment: that is why we call this phase the (T') phase. Indeed, like in the case of core-shell nanodots, the existence of such a nonzero toroidal moment induces strains. However, for core-shell nanowires, we calculated (not shown) that only a normal strain is observed (zero shear strain components), with a high contribution of  $g_z$  to the strain along the  $z$  direction and a weaker contribution on the  $x$  and  $y$  directions: a global elongation of the nanowires is therefore observed. That is why we use a prime in (T') notation because this phase is different

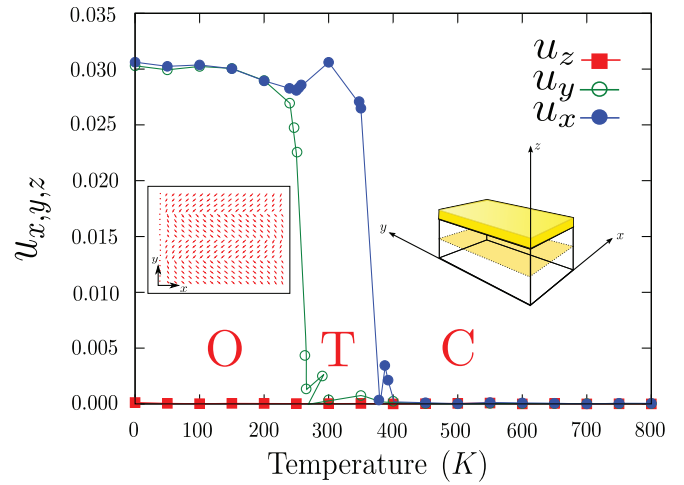


FIG. 8. (Color online) Temperature dependence of the component of local modes in the case of a ceramic constituted of core-shell nanoplanes; at low temperature, only in-plane  $x$  and  $y$  components are observed. Whatever the temperature is, no component of toroidal moment is ever observed. In insert, stripes pattern of polarization observed in the orthorhombic plane.

from the (T) phase of bulk BT. At higher temperature, as both polarization and toroidal moment disappear at the same temperature, a direct transition (T')-(C) is observed, which means that no (C') phase is observed.

### C. Case of nanoceramics constituted of infinite core-shell nanoplanes

This case is physically relevant for composites constituted of stacking of ultrathin films surrounded by dead layers. In this case, the calculation shows that no toroidal moment ever exists: this is intuitively understandable as a depolarizing field (which tends to destroy ferroelectricity) only happens along the  $z$  axis perpendicular to the plane. The temperature dependence of polarization (see Fig. 8) shows two equal components along  $x$  and  $y$  axes below  $\approx 250$  K, i.e., an (O) orthorhombic phase, similar to that of bulk BT, as no supplementary strain is present; between  $\approx 260$  and  $\approx 360$  K, only one  $x$  axis (or  $y$  axis) component is observed, i.e., a (T) tetragonal phase. Above  $\approx 360$  K, a paraelectric phase occurs, which is a “true” cubic phase (contrary to the nanodots case), as no strain occurs at these temperatures.

However, although no vortex is ever observed, in the low-temperature orthorhombic phase, a peculiar pattern of the local polarization is still observed. Indeed, when planes of the core parallel to the shell planes are uniformly polarized, perpendicular planes reveal alternation of stripes with opposite direction of polarization (insert of Fig. 8). This type of patterns have already been evidenced in a very thin film of  $\text{PbTiO}_3$ <sup>16</sup> and are explained by the interplay between strain and the amount of screening of surface charges.<sup>17</sup> Clearly, this situation and the situation in core-shell nanoplanes are very similar.

## IV. DISCUSSION

In the first part of this section, we address the comparison of our results with the situation of isolated nanodots as calculated

in Refs. 12 and 13. In the second part, we pay attention to the picture of nanoceramics from previous results obtained in the framework of the Landau theory. In the last part, a new Landau-based formalism, using a toroidal moment as order parameter is proposed and a new phase diagram is predicted.

#### A. Comparison of core-shell nanodots ceramics with the case of isolated nanodots

As shown in the previous section, ceramics based on core-shell nanodots display in certain ranges of shell thickness or shell permittivity, a local organization of polarization in the form of vortices, below a critical temperature. Such organization was evidenced and developed in many examples by several authors, in the case of isolated nanodots submitted to a depolarization field.<sup>12,13</sup> In these examples, the surface of the dots is elastic-free, whereas in our modeling, we use periodic boundary conditions that create on the surface a certain strain in addition to the depolarization field. In the framework of isolated dots, the depolarization field was introduced via the relation

$$\varepsilon_{\text{Heff}(p_i, V_i, \eta)}^{\text{Tot}} = \varepsilon_{\text{Heff}(p_i, V_i, \eta)} + \beta \sum_i \langle E_d \rangle p_i, \quad (2)$$

which represents the total energy of the dots decomposed into two terms: the first one is the energy associated to the dot put in void, which is a function of polarization  $p_i$ , homogeneous  $\eta$ , and inhomogeneous  $V_i$  strain, which therefore is completely submitted to depolarizing field  $E_d$ , and the second term, which is negative, “tunes” via the  $\beta$  coefficient the effect of this field: (i) when  $\beta = 1$ , the depolarizing field is completely screened, and the dot is therefore in short-circuit, and (ii) when  $\beta = 0$ , the depolarizing field is completely applied. Different authors have shown that the ground state of stress-free ferroelectric nanodots consists of a vortex structure that does not exhibit any polarization but an electric toroidal moment for  $\beta$  values smaller than 0.95, in order to completely annihilate the depolarizing field. On the other hand, for  $\beta > 0.95$ , such nanodots possess a polarization whose magnitude strongly depends on  $\beta$  as well as on the dots’ size, because the depolarizing field increases in magnitude and thus opposes more strongly against the polarization. Moreover, it was shown that most of experimental situations could be accurately reproduced with a  $\beta$  value of  $\approx 0.97$ . However, it should be noted that the case  $\beta = 1$  (short circuit) does not correspond to an infinite crystal: indeed, whereas a ferroelectric polarization with no toroidal moment is observed, in a similar situation to infinite crystal, in the case of BT, no orthorhombic phase was observed (as it is experimentally observed in bulk BT) and the critical temperatures of the other phases transitions are strongly depressed. This is due to the fact that the dots in this case are put in void, and therefore no elastic interaction exists between the surface and the outside environment. This type of modeling aims at dealing (for  $\beta \neq 1$ ) with the physical situation of isolated nanodots with screened charges (because of humidity or dust) or inner conductivity (with a dead layer or conductivity at the surface but not with a core-shell structure). That is why differences, in particular, in the phase sequences, the critical temperature, the coexistence of vortices and polarization, exist with our modeling. However, many qualitative similarities do

exist, in particular, the possibility of coexistence of vortices with homogeneous polarization.

#### B. Comparison of core-shell nanodots ceramics with the case of ferroelectric composites

Another approach has been performed to explain the existence of vortices: the so-called phase-field simulation<sup>18</sup> in which the authors decomposed the particle into small cells in which a Landau potential is numerically minimized, assuming of course boundaries continuity. By iteration, the total free energy of the particle could be minimized. In the case of a nanodot, these authors observed a polarization pattern in the form of vortex; however, in the case of nanowires, they did not observe vortices as we have observed but a sole polarization along the wire axis.

We should also mention that some authors have considered the case of nanocomposites constituted of nanowires embedded in a matrix. Prosandeev and Bellaiche<sup>16,19</sup> have considered the case of PbZrO<sub>3</sub>-PbTiO<sub>3</sub> (with 50-50 composition) material and applied a coefficient of “ferroelectric strength” as a parameter. This leads to situations where either the dots or the matrix is PZT, the other part been a PZT material with different ferroelectric properties. The authors could observe in their phase diagram the occurrence of vortices that can coexist with polarization. However, two important differences with our study are the facts that the permittivity of the shell in our case is frozen and not allowed to change with temperature or any other parameters, and that we have considered a core and a shell with different mechanical properties: in particular, paying special attention to the temperature dependence of strains (which was not done in Ref. 19) allowed us to evidence new phases. Our paper being less general than Prosandeev and Bellaiches’ paper allowed us to have a more complete description of the situation encountered in the case of nanoceramic, to calculate quantitative values of temperature dependence of polarization, toroidal moment, permittivity, etc., to easily play with the size of the nanodots, the shell thickness, permittivity, etc.

Another study<sup>20</sup> by the same team has considered the case of nanocomposites constituted of nanowires embedded in a matrix of a paraelectric or a ferroelectric material, which is not really a core-shell situation, as the equivalent value of  $\alpha$  is in this case  $18/12 = 1.5$ , that is, much higher than in our case. Very rich pattern situations have been observed, among them a similar situation in which vortices coexist with a polarization along the normal axis of the wire.

#### C. Comparison with the Landau theory of nanoparticles

We have very recently published a Landau theory of core-shell nanoceramics.<sup>11</sup> This was done by solving first the Laplace equation for a single core-shell particle (for different cases of isotropic or anisotropic shapes) submitted in void to an external electric field. Then, the case of ceramics is obtained by placing the particle in the effective medium field, which averages the effects of all surrounding particles to obtain in a self-consistent way the equations for the different internal electric fields, the permittivity and the polarization of a nanoceramic constituted of such core-shell particles. In particular, we found that the component of the core electrical

field  $E_i$  and of the core-shell total polarization  $P_{Si}$  are

$$\begin{aligned} E_i &= \beta_i \frac{P_i}{\varepsilon_0} + \gamma_i E_{\text{app},i}, \\ P_{S_i} &= \beta'_i P_i + \gamma'_i E_{\text{app},i}, \end{aligned} \quad (3)$$

with  $i = x, y, z$ ,  $P_i$ , and  $E_{\text{app},i}$  the components of the core polarization and of the external applied field, respectively. One can see that the core electric field  $E_i$  and the total polarization  $P_i$  are proportional to  $\beta_i$ ,  $\gamma_i$  and  $\beta'_i$ ,  $\gamma'_i$  coefficients, respectively; these four coefficients are simple fractional functions of  $\alpha$  and  $\varepsilon_r$ . In the case of spherical core-shell particles,  $\beta_x = \beta_y = \beta_z = \beta$ , as well as for the other coefficients. One should notice that the  $\beta$  coefficient, although of a very close physical significance, is numerically different from the one used in the *ab initio* calculations (2) as it goes from 0 in short-circuit conditions, i.e., in bulk, to 1/3 in open circuit conditions, i.e., in an isolated spherical dot. For instance, as we will use latter this coefficient, we have for a sphere,<sup>11</sup>

$$\beta_{i=x,y,z} = \frac{1 - \alpha^3}{[(2\alpha^3 + 1)\varepsilon_2 + \alpha^3 - 1]}. \quad (4)$$

We have introduced afterwards the expression of the core-shell polarization into the Landau potential for a single crystal<sup>21</sup> in which we added a depolarizing energy as well as an energy associated to the effect of an external field [two last terms in Eq. (5) below], which allowed us to get the phases diagrams for different cases of nanoparticles shapes. Thus we found

$$\begin{aligned} F_p &= \alpha_1^*(T)(P_1^2 + P_2^2 + P_3^2) + \alpha_{11}(P_1^4 + P_2^4 + P_3^4) \\ &+ \alpha_{12}^*(P_1^2 P_2^2 + P_2^2 P_3^2 + P_3^2 P_1^2) + \alpha_{111}(P_1^6 + P_2^6 + P_3^6) \\ &+ \alpha_{112}[P_1^2(P_2^4 + P_3^4) + P_2^2(P_1^4 + P_3^4) + P_3^2(P_1^4 + P_2^4)] \\ &+ \alpha_{123}P_1^2 P_2^2 P_3^2 + \alpha_{1111}(P_1^8 + P_2^8 + P_3^8) \\ &+ \alpha_{1112}[P_1^6(P_2^6 + P_3^2) + P_2^6(P_1^2 + P_3^2) + P_3^6(P_1^2 + P_2^2)] \\ &+ \alpha_{1122}(P_1^4 P_2^4 + P_2^4 P_3^4 + P_1^4 P_3^4) \\ &+ \alpha_{1123}(P_1^4 P_2^2 P_3^2 + P_2^4 P_1^2 P_3^2 + P_3^4 P_1^2 P_2^2) \\ &+ \sum_i -\frac{\beta_i P_i^2}{2\varepsilon_0} - P_i \gamma_i E_{\text{app},i}. \end{aligned} \quad (5)$$

Neither strain nor coupling between polarization and strain were needed to explain the properties of the core-shell ceramic: the core-shell picture of nanoparticles adequately explains the size evolution of the critical temperatures and the phase sequences. Of course, surface tension or strain can play a role, but at a primary stage they are not needed to describe experimental data.<sup>11</sup> Numerical minimization of the  $F_p$  Landau potential results for instance in curves of polarization versus external electric field, which were numerically integrated to obtain the maximum density of energy that can be stored in the nanoceramic. These calculations were performed in the case of different shapes of nanoparticles.

In the case of spherical core-shell nanoparticle ceramics, which is the closest case to that of nanodots, we have obtained within this Landau theory a phase diagram in which all bulk phases of BT [(C), (T), (O), and (R) phases] are observed for a weak value of  $\alpha$  shell thickness, the three ferroelectric

critical temperatures being shifted downwards from the same negative amount, with increasing value of  $\alpha$ . At higher values of  $\alpha$ , the 3 ferroelectric phases successively disappear and finally only the cubic phase is observed down to the lowest temperatures. Of course, this Landau theory fails to predict the existence and the peculiar properties of the (C') phase, due to the existence of vortices. This is therefore a point that should be addressed in a more efficient Landau theory. In Fig. 9 (top), we have superimposed these Landau phase diagrams with the results of our *ab initio* derived effective Hamiltonian calculations. These calculations (see Sec. III A) have indeed shown also the cancelation of any ferroelectric phase at the lowest reachable value of  $\alpha = 1.035$  (dotted white line) and were able to predict the existence of the (C')-(C) transition as well as its critical temperature (white square), which happened to be size independent. However, the *ab initio* calculations fail to capture the physics at small shell thickness and/or high permittivity, in particular, the existence of the three ferroelectric phases.

We have also studied by the Landau theory the case of nanorods and its limit case, i.e., nanowires: for an increasing anisotropy of the nanoparticles, the (T) phase is stabilized against the two other ferroelectric phases, which is a rather intuitive result. In the case of nanowires, the Landau theory predicts a sole (T)-(C) transition [no more (R) and (O) ferroelectric phases] with a critical temperature independent of the coating thickness  $\alpha$ . Superimposing these results with the *ab initio* derived effective Hamiltonian results (see Fig. 9 middle) leads to the fact that the (T) phase is a (T') phase, which transforms at a temperature independent of the shell thickness  $\alpha$  towards the (C) cubic phase. The same limitation for both types of modeling is observed: the Landau theory failed to predict the existence of vortices inside the tetragonal phase [(T') phase], whereas the *ab initio* derived effective Hamiltonian calculations cannot operate at very low values of  $\alpha$ . However, in this case, no change is predicted by the Landau theory, and the agreement between both types of modeling in the  $\alpha$  range where they can be compared is rather fair: not only for the critical temperature values (white triangles to be compared with the T'-C line) but also for the value of the temperature dependence of the polarization calculated by both methods (insert of Fig. 9 middle).

We have also studied in the Landau theory the case of nanodisks: for an increasing anisotropy of the nanoparticles, the (T) and (O) phases are stabilized against the (R) ferroelectric phase; this is again a rather intuitive result, and at the limit of "infinite anisotropic nanodisks," we get the case of nanoplanes. In this case, the Landau theory predicts a cancelation of the (R) phase, the orthorhombic phase being stable down to the lowest temperature, whatever  $\alpha$  is, and (O)-(T) and (T)-(C) transitions with critical temperatures independent of  $\alpha$ . Superimposing these results with the *ab initio* derived effective Hamiltonian results (see Fig. 9, bottom) leads to a rather fair agreement regarding the two critical temperatures calculated by both methods (white triangles and circles, and solid lines), as well as for the temperature dependence of the polarization (see an insert of Fig. 9, bottom). A limitation of the *ab initio* calculations is again the fact that it cannot operate at very low values of  $\alpha$ , which is also in this case less important, as no change is predicted by the Landau theory.

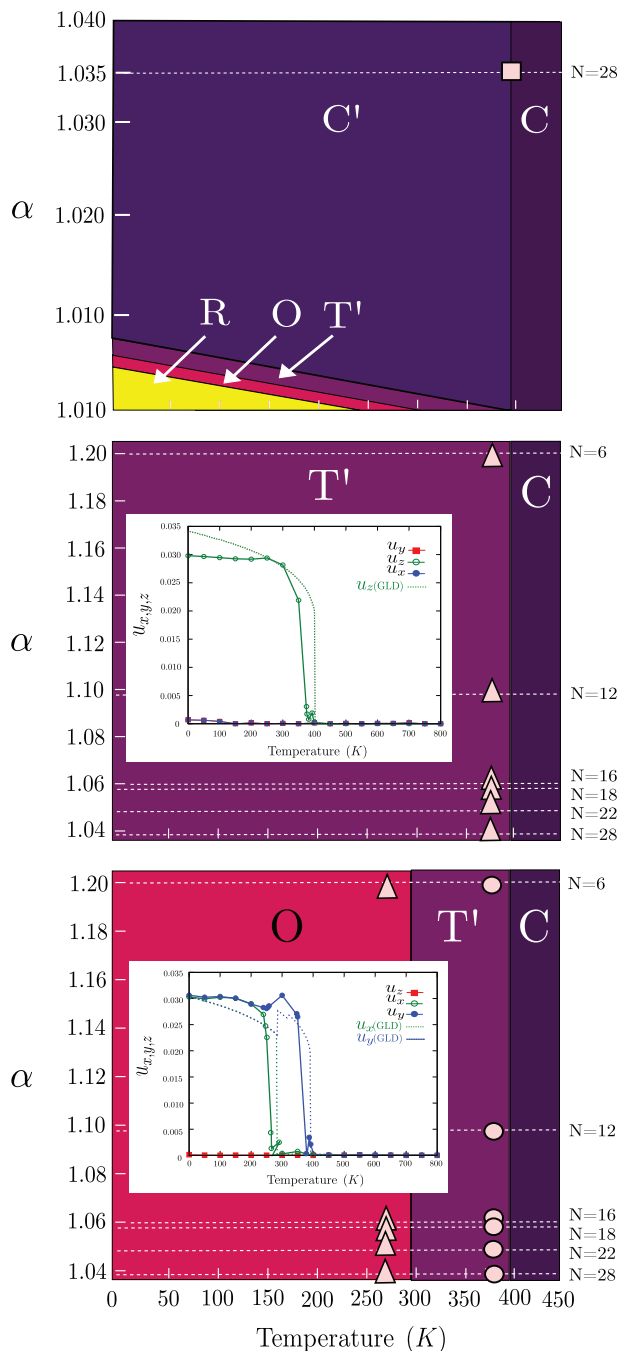


FIG. 9. (Color online) (Top) Shell thickness-temperature phase diagram of a ceramic constituted of core-shell nanodots with shell permittivity  $\epsilon_r = 5$ , built from an *ab initio* derived effective Hamiltonian and Landau theory. (Middle) Same but for a ceramic constituted of core-shell nanowires; in the insert, we show the calculated polarization from first principles and Landau theory. (Bottom) Same for a ceramic constituted of core-shell nanoplanes; in the insert, we show the calculated polarization by *ab initio* and Landau theory.

**D. Toroidal moment of core-shell nanodots ceramics and the building of a new Landau theory**

Many authors have pointed out that the toroidal moment as defined above is an order parameter of ferroelectric transitions at nanosizes. Although a detailed analysis of symmetry

associated with this new order parameter in relation to the symmetry of the electrostatic forces is still lacking, one may wonder if it could be used to build a Landau theory of core shell that could take into account the results we have obtained in Sec. III, in particular, the existence of vortices, the possible coexistence with polarization, etc., and possibly predict new ones. This should have also the advantage to provide results in the whole range of shell thickness  $\alpha$  and permittivity  $\epsilon_r$ , which is unreachable by *ab initio* derived effective Hamiltonian calculations, due to computational limitations. Landau theory of course is a thermodynamic theory and deals, therefore, in the case of such compounds as BT, only with macroscopic polarization. Thus in most of the situations, local and macroscopic polarizations are not identical (except in highly homogeneous cases); for instance, one can imagine two very different situations with both macroscopic polarizations equal to zero: one with a lattice of vortices, and another one where the local polarization is fully disordered. These two situations will have different entropy, different specific heat, etc. Thus the toroidal moment does not directly depend on the thermodynamic polarization  $P$ . Another way to say this is that a thermodynamic potential with only  $P$  as an order parameter cannot describe many situations, which could be described with a potential that includes  $G$  and  $P$  even in a phase-field simulation, see Sec. IV B. The relationship between  $P$  and  $G$  should be introduced via coupling terms in the potential, just like when using polarization and strain, although these two latter quantities are also strongly related and both depend on the atomic positions and can be calculated from them; in that sense, they are not independent variables.

Here, we propose to follow such a demarche in order to build a preliminary and simplified model. First of all, in our opinion, the possibility to build such Landau theory arises from the fact that a system with polarization vortices can be considered as a homogeneous system from the stand point of its energy. Indeed (not shown), the electric field and the local polarization (i.e., the local mode) are always parallel: this minimizes the electrostatic energy  $E_P$ , just like in an infinite crystal with homogeneous (i.e., constant) polarization. Moreover, the local modes have amplitude, which is constant inside the vortices, except close to the boundaries of the dots. This means that the electrostatic energy of a vortex should be considered as homogeneous. The same remark applies for the elastic energy associated to the configuration of the local mode. Therefore the behavior and properties of a system with vortices should be very close to a homogeneous system, if we replace the polarization by the volume average of the norm of the individual dipolar moment which constitutes the toroidal moment  $g$ .

We must now consider some conditions that must be addressed by the Landau potential using  $g$  as an order parameter. (1) It must have a similar form as the potential that uses polarization as the order parameter. (2) As there is no long-range dipole-dipole interaction between cells, the energy associated to  $g$  is not strongly modified by the existence of the other cells: in other words, the energy is not modified by the boundary conditions, whatever they are in short or open circuits. (3) As previously shown,  $g$  is decreasing with temperature and has a critical temperature close to the Curie temperature  $T_C$  of bulk BT: this is a result from the *ab initio*

derived effective Hamiltonian calculations; we can therefore include a  $(T - T_C)(g_1^2 + g_2^2 + g_3^2)$  term. (4) For high shell thickness, the three components  $g_1$ ,  $g_2$ , and  $g_3$  of  $g$  are equal or almost equal below  $T_C$ , which implies weak interactions between themselves [such as  $g_1^2(g_2^2 + g_3^2)$ ], thus we can neglect them but include terms such as  $(g_1^4 + g_2^4 + g_3^4)$ , etc. (5) A  $g_i$  component is weakly affected by a  $P_i$  component of polarization but is more drastically changed if the other components of polarization exist: therefore we must include components of the form  $g_1^2(P_2^2 + P_3^2)$  and  $P_1^2(g_2^2 + g_3^2)$ , but we can neglect terms such as  $g_1^2(P_1^2 + \dots)$ . (6) *Ab initio* calculations have shown a  $\sigma$  strain associated with the existence of  $g$ , thus we must put an interaction term between  $g$  and  $\sigma$ .

This leads to the addition of new terms in the  $F_P$  Landau potential (5) associated to  $P$  polarization such as to form the complete  $F_{G+P}$ :

$$\begin{aligned}
F_{G+P} = & F_P + \alpha'_1(T - T_C)(g_1^2 + g_2^2 + g_3^2) + \alpha'_{11}(g_1^4 + g_2^4 + g_3^4) \\
& + \alpha_{111}(g_1^6 + g_2^6 + g_3^6) \\
& + \alpha'_{12}[P_1^2(g_2^2 + g_3^2) + P_2^2(g_1^2 + g_3^2) + P_3^2(g_1^2 + g_2^2)] \\
& + \alpha''_{12}[g_1^2(P_2^2 + P_3^2) + g_2^2(P_1^2 + P_3^2) + g_3^2(P_1^2 + P_2^2)] \\
& + \alpha'_{123}[g_1^2 P_1^2 + g_2^2 P_2^2 + g_3^2 P_3^2] \\
& + \alpha_{1122}(P_1^4 P_2^4 + P_2^4 P_3^4 + P_1^4 P_3^4) \\
& + \alpha_{1123}(P_1^4 P_2^2 P_3^2 + P_2^4 P_1^2 P_3^2 + P_3^4 P_1^2 P_2^2) \\
& - Q'_{11}(\sigma g_1^2 + \sigma_2 g_2^2 + \sigma_3 g_3^2) \\
& - Q'_{12}[\sigma_1(g_2^2 + g_3^2) + \sigma_2(g_1^2 + g_3^2) + \sigma_3(g_1^2 + g_2^2)] \\
& - Q'_{44}(g_2 g_3 \sigma_4 + g_1 g_3 \sigma_5 + g_2 g_1 \sigma_6) \quad (6)
\end{aligned}$$

in which the order parameters ( $P$  and  $g$ ) compete with each other.

For the  $F_P$  polarization part of the  $F_{G+P}$  Landau potential, all the  $\alpha_{ij}$  etc and  $Q_{ij}$  coefficients have already been published for bulk BT (see Table I). In order to get all additional terms of Eq. (6) (terms with prime), we have proceeded in a practical way, although not mathematically correct: we started by taking the same values as in the  $F_P$  expansion and empirically modified them to get the  $\alpha'_{ij}$  etc and  $Q'_{ij}$  (see Table II) coefficients able to reproduce the results already obtained in the situations described above by the *ab initio* derived effective Hamiltonian calculations shown in the preceding sections. This is shown on Fig. 10 for core-shell nanodots, and we did also the same work for nanowires (not shown). This does not of course guarantee that other sets of parameters could not work as well but this is the first basic attempt, which should be more deeply and systematically investigated in a further study.

Now we can also use this potential to predict new results, which may involve vortices and thus are not reachable in the “classical” Landau theory, in particular, for the case of small thickness and high permittivity of shell, which are unreachable by *ab initio* calculations.

We have explored the whole range of thickness and permittivity of shell and built a new phase diagram (see Fig. 11) versus screening coefficient  $\beta$  from Eq. (3) and temperature;

TABLE II. Landau coefficient used in the expansion of free energy vs polarization and toroidal moment.

$F_P$ coefficients		$F_G$ coefficients	
	Value		Value
$\alpha_1(T)$	$4.124 \times 10^5 (T-115)$	$\alpha_1(T)'$	$4.124 \times 10^5 (T-100)$
$\alpha_{11}$	$-2.097 \times 10^8$	$\alpha'_{11}$	0
$\alpha_{12}$	$7.974 \times 10^8$	$\alpha'_{12}$	$23.922 \times 10^8$
$\alpha_{111}$	$1.294 \times 10^9$	$\alpha'_{111}$	$1.294 \times 10^{10}$
$\alpha_{112}$	$-1.956 \times 10^9$		
$\alpha_{123}$	$-2.5 \times 10^9$		
$\alpha_{1111}$	$3.863 \times 10^{10}$		
$\alpha_{1112}$	$2.529 \times 10^{10}$		
$\alpha_{1122}$	$1.637 \times 10^{10}$		
$\alpha_{1123}$	$1.367 \times 10^{10}$		
		$\alpha''_{12}$	$23.922 \times 10^8$
		$Q'_{11}$	0.0275
		$Q'_{12}$	-0.0108
		$Q'_{44}$	0.0147
		$s_{11}$	$8.3 \times 10^{12}$

as previously shown, this coefficient is a simple function of  $\alpha$  and  $\varepsilon_r$  [see Eq. (4)]. This gives a more general form for the phase diagram, as several couples  $(\alpha, \varepsilon_r)$  can give the same value of  $\beta$ ; however, we also plot an  $\alpha$  scale for the case  $\varepsilon_r = 70$  in order to give an idea of the high-permittivity situation. On the same figure, we compare with the phase diagram obtained from the “conventional” Landau theory of Fig. 9 upper part (dashed lines). Several important features in this diagram and differences with the previous diagram of Fig. 9 can be observed. (1) A supplementary (C')-(C) transition occurs whatever  $\beta \neq 0$  (or  $\alpha \neq 1$ ) is, at the same  $T_C$  temperature. (2) Vortices are observed in two phases, i.e., the ferroelectric (T') and the nonferroelectric (C') phases. (3)

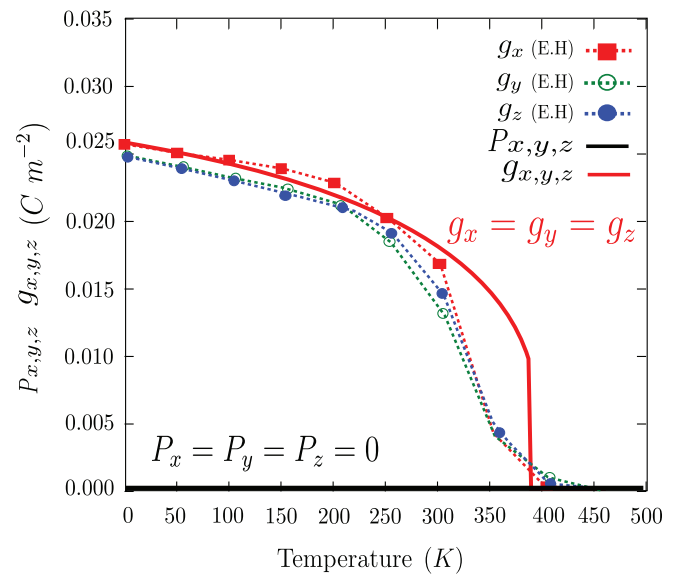


FIG. 10. (Color online) Temperature dependence of the components of polarization and toroidal moment in the case of a ceramic constituted of core-shell nanodots calculated from first principles (dotted lines) and Landau theory using  $g$  and  $P$  as order parameters (solid line).

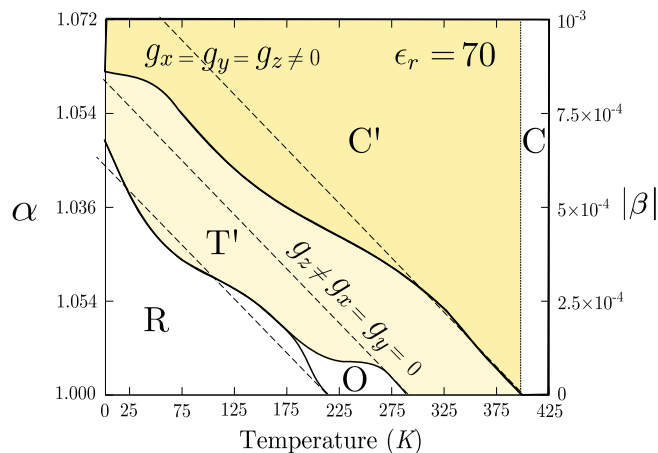


FIG. 11. (Color online) Phase diagram vs screening coefficient  $\beta'$  (which is a simple function of  $\alpha$  and  $\epsilon_r$ ) and temperature. We have also put an  $\alpha$  scale for the case  $\epsilon_r = 70$  in order to give an idea of the high-permittivity situation. In the same figure, we compare with the phase diagram obtained from the “conventional” Landau theory of Fig. 9 upper part (dashed lines).

For high values of  $\beta > \approx 8.5 \cdot 10^{-4}$ , the ground state is at low temperature, the nonferroelectric ( $C'$ ) phase in which vortices are observed. (4) At weak values of  $\beta$ , the succession of three ferroelectric phases (R), (O), ( $T'$ ) is observed and the ( $T'$ ) phase is not observed. (5) The (O) orthorhombic phase has only a small  $\beta$  range of existence (contrary to the diagram of Fig. 9) and disappears above  $\beta \approx 1.3 \cdot 10^{-4}$ . Above this value, a direct (R)-( $T'$ ) transition is observed. (6) A deviation of the critical lines from linearity occurs, in particular, for the ( $T'$ )-( $C'$ ) line.

From the Landau expansion, we can also calculate the permittivity of the ceramic. In particular, if we calculate it at high value of  $\alpha$ , i.e., in the range of the phase diagram where no ferroelectric phase happens, for instance,  $\alpha = 1.02$ , a clear and strong peak appears at the temperature of the ( $C'$ )-(C) (nonpolar) transition (see Fig. 5 dotted line). This result confirms the attribution of the peaks observed in the temperature dependence of permittivity obtained in *ab initio* calculations (see Fig. 5). The appearance of this peak is thus clearly not associated with the onset of ferroelectricity but is the consequence of the vanishing (on cooling) or onset (on heating) of the toroidal moment, via the coupling of both order parameters in Eq. (6).

## V. CONCLUSION

We have emphasized the fact that many experimental properties of nanoceramics can be explained by the existence of a core-shell structure of the nanograins. In this framework, we have studied BaTiO<sub>3</sub> ceramics constituted of core-shell nanoparticles by using *ab initio* derived effective Hamiltonian calculations whose application range is for large values of shell thickness and low values of shell permittivity. When the nanoparticles are core-shell isotropic nanodots, no ferroelectric phase emerges but a well-defined organization of the local polarization occurs, in the form of vortices, below a critical temperature as found by Naumov *et al.*<sup>12</sup> in the case of isolated dots. We have shown that vortices

induce several new features, e.g., a supplementary phase transition from the paraelectric cubic phase of BaTiO<sub>3</sub> towards a nonpolar rhombohedral phase with a strong anomaly of permittivity in the form of a peak associated to this transition, a destabilization of the orthorhombic phase, etc. The calculation has been extended to the case of ceramics constituted of core-shell nanowires and nanoplanes. In the former case, axial polarization coexists below a critical temperature with planar vortices in a ferroelectric tetragonal phase; in the latter case, no vortex is ever observed, but the rhombohedral ferroelectric phase of bulk BT is suppressed: only orthorhombic-tetragonal-cubic phases are observed, however, in the low-temperature orthorhombic phase, the polarization adopts a peculiar organization in the form of stripes rather than a conventional domain configuration.

We have afterwards compared these results with the situation of isolated nanodots and of nanocomposites as studied by Bellaïches' team.<sup>12,19,20</sup> The first result is that there are many similar points in both studies of nanoceramics and of nanodots: despite the presence of stress and of a linear dielectric as a shell, the system is essentially sensitive to the depolarizing field and thus shares a close behavior with nanodots. However, we should stress that contrary to nanodots, our study focuses on a nanoceramics description and therefore we stress the details that are not available in common nanodot studies (strain, permittivity of the shell/matrix, nature of the shell/matrix, the necessity to mimic realistic materials in both their electric and mechanic properties, the effect of size of the dot /thickness of the coating and its dielectric permittivity, the dielectric permittivity of the nanoceramic, etc.). Also, there are many differences and new features, e.g., a phase with coexistence of both vortices and homogeneous perpendicular polarization, and a new transition from cubic paraelectric phase towards nonpolar rhombohedral phase. Also, to the best of our knowledge, anomalies in dielectric permittivity (see Fig. 5) associated with the onset of a toroidal moment have never been evidenced before; in the case of core-shell nanowires, we have demonstrated a new tetragonal phase.

Our results have also been compared with those obtained by the Landau theory of core-shell ceramics we have recently published.<sup>11</sup> A very good agreement regarding the stability and critical temperature of ferroelectric phases was observed in the range where both theories can be compared. However, the *ab initio* calculations fail to capture the physics at small-shell thickness and/or high-shell permittivity, whereas the Landau theory fails to predict the peculiar property of the phases in which vortices exist.

Therefore, in a tentative way to build a global theory, we have constructed a new Landau potential using both the polarization and the toroidal moment as order parameters, which allowed us to propose a new phase diagram, whatever the shell thickness and permittivity are. This phase diagram displays and predicts many new properties such as new phases where vortices occur or the cancelation of the orthorhombic phase at high shell thickness, etc.; the temperature dependence of the polarization, toroidal moment, permittivity, etc., could be also calculated. Although this potential is only a preliminary proposition and a more rigorously built potential is still to be written, we believe, however, that it captures the most important features of the core-shell ceramics.

Comparison of our results with the experimental situation is unfortunately rather difficult and indirect. Regarding the phase sequence, Lin *et al.*<sup>21</sup> observed at nanosizes rhombohedral and orthorhombic phases as we observed. Also, Buscaglia *et al.*<sup>22</sup> and Schalg *et al.*<sup>23</sup> have observed at small sizes, a cubic phase but with a local polar structure: although they could not describe this polar order, it could be related to our finding of the C' phase. Aoyama *et al.*<sup>24</sup> have observed a "quasirhombohedral phase," which is also compatible with our finding of the C' phase. Regarding the vortices they have been observed in PZT films<sup>25</sup> and PZT micrometer-sized ferroelectric capacitors,<sup>26</sup> also in BFO films,<sup>27</sup> the same observations were made in bulk single crystal of BT.<sup>28</sup> On the contrary, Polking *et al.*<sup>29</sup> observed in nanodots of BT and GeTe, linear polarization down to 5 nm. That is to say, to

our knowledge, no vortex could be experimentally detected in free ferroelectric nanodots; the same applies in the case of a nanoceramic, which is a case even harder to be dealt with experimentally. This is why we are now trying such a study in BT nanoceramics in order to test our results. But many difficulties will have to be tackled in a ceramic, in particular, the possible conduction of the grains and its inhomogeneity, also their size inhomogeneity, which should create an averaging that could mask some effects. That is why we must try to use ideally monodisperse nanograins.

#### ACKNOWLEDGMENTS

M.A. and J.M.K. want to thank Dr. Bellaiche and Dr. Pertsev for many very useful discussions.

- 
- <sup>1</sup>T. Hoshina, S. Wada, Y. Kuroiwa, and T. Tsurumi, *Appl. Phys. Lett.* **93**, 192914 (2008).
- <sup>2</sup>M. T. Buscaglia, M. Viviani, V. Buscaglia, L. Mitoseriu, A. Testino, P. Nanni, Z. Zhao, M. Nygren, C. Harnagea, D. Piazza, and C. Galassi, *Phys. Rev. B* **73**, 064114 (2006).
- <sup>3</sup>J. Carreaud, P. Geimeiner, J. M. Kiat, B. Dkhil, C. Bogicevic, T. Rojac, and B. Malic, *Phys. Rev. B* **72**, 174115 (2005).
- <sup>4</sup>J. Carreaud, C. Bogicevic, B. Dkhil, and J. M. Kiat, *Appl. Phys. Lett.* **92**, 242902 (2008).
- <sup>5</sup>J. M. Kiat, C. Bogicevic, F. Karolak, G. Dezanneau, N. Guiblin, W. Ren, L. Bellaiche, and R. Haumont, *Phys. Rev. B* **81**, 144122 (2010).
- <sup>6</sup>J. Carreaud, J. M. Kiat, B. Dkhil, M. Alguero, J. Ricote, R. Jimenez, J. Holc, and M. Kosec, *Appl. Phys. Lett.* **89**, 252906 (2006).
- <sup>7</sup>J. M. Kiat, C. Bogicevic, P. Gemeiner, A. Al-Zein, F. Karolak, N. Guiblin, F. Porcher, B. Hehlen, L. Yedra, S. Estrade, F. Peiro, and R. Haumont, *Phys. Rev. B* **87**, 024106 (2013).
- <sup>8</sup>A. Bassano, V. Buscaglia, M. Sennour, M. T. Buscaglia, M. Viviani, and P. Nanni, *J. Nanopart. Res.* **12**, 623 (2010).
- <sup>9</sup>U.-C. Chung, C. Elissalde, F. Momprou, J. Majimel, S. Gomez, C. Estourne, S. Marinel, J. A. Klein, F. Weill, D. Michau, S. Mornet, and M. Maglione, *J. Am. Ceram. Soc.* **93**, 865 (2010).
- <sup>10</sup>A. Y. Emelyanov, N. A. Pertsev, S. Hoffman-Eifert, U. Bottger, and R. Waser, *J. Electroceram.* **9**, 5 (2002).
- <sup>11</sup>M. Anoufa, J. M. Kiat, I. Kornev, and C. Bogicevic, *J. Appl. Phys.* **113**, 054104 (2013).
- <sup>12</sup>I. I. Naumov, L. Bellaiche, and H. Fu, *Nature (London)* **432**, 737 (2004).
- <sup>13</sup>I. Ponomareva, I. I. Naumov, and L. Bellaiche, *Phys. Rev. B* **72**, 214118 (2005).
- <sup>14</sup>S. Prosandeev and L. Bellaiche, *Phys. Rev. Lett.* **97**, 167601 (2006).
- <sup>15</sup>W. Zhong, D. Vanderbilt, and K. M. Rabe, *Phys. Rev. Lett.* **73**, 1861 (1994).
- <sup>16</sup>S. K. Streiffer, J. A. Eastman, D. D. Fong, Carol Thompson, A. Munkholm, M. V. Ramana Murty, O. Auciello, G. R. Bai, and G. B. Stephenson, *Phys. Rev. Lett.* **89**, 067601 (2002).
- <sup>17</sup>Igor Kornev, Huaxiang Fu, and L. Bellaiche, *Phys. Rev. Lett.* **93**, 196104 (2004).
- <sup>18</sup>J. Wang, M. Kamlah, T. Y. Zhang, Y. Li, and L. Q. Chen, *Appl. Phys. Lett.* **92**, 162905 (2008).
- <sup>19</sup>S. Prosandeev and L. Bellaiche, *J. Mater. Sci.* **44**, 5235 (2009).
- <sup>20</sup>L. Louis, I. Kornev, G. Geneste, B. Dkhil, and L. Bellaiche, *J. Phys.: Condens. Matter* **24**, 402201 (2012).
- <sup>21</sup>S. Lin, T. Lu, C. Jin, and X. Wang, *Phys. Rev. B* **74**, 134115 (2006).
- <sup>22</sup>V. Buscaglia, M. T. Buscaglia, M. Viviani, T. Ostapchuk, I. Gregora, J. Petzelt, L. Mitoseriu, P. Nanni, A. Testino, R. Calderone, C. Harnagea, Z. Zhao, and M. Nygren, *J. Eur. Ceram. Soc.* **25**, 3059 (2005).
- <sup>23</sup>S. Schlag and H. F. Eicke, *Solid State Commun.* **91**, 883 (1994).
- <sup>24</sup>M. Aoyama, T. Hasegawa, N. Ogita, N. Nakajima, H. Maruyama, H. Kurokawa, and M. Udagawa, *Chin. J. Phys.* **49**, 49 (2011).
- <sup>25</sup>C. L. Jia, K. W. Urban, M. Alexe, D. Hesse, and I. Vrejoiu, *Science* **331**, 1420 (2011).
- <sup>26</sup>A. Gruverman, D. Wu, H.-J. Fan, I. Vrejoiu, M. Alexe, R. J. Harrison, and J. F. Scott, *J. Phys.: Condens. Matter* **20**, 342201 (2008).
- <sup>27</sup>N. Balke, B. Winchester, W. Ren, Y. H. Chu, A. N. Morozovska, E. A. Eliseev, M. Huijben, R. K. Vasudevan, P. Maksymovych, J. Britson, S. Jesse, I. Kornev, R. Ramesh, L. Bellaiche, L. Q. Chen, and S. V. Kalinin, *Nat. Phys.* **8**, 81 (2012).
- <sup>28</sup>R. G. P. McQuaid, L. J. McGilly, P. Sharma, A. Gruverman, and J. M. Gregg, *Nat. Commun.* **2**, 404 (2011).
- <sup>29</sup>M. J. Polking, M. G. Han, A. Yourdkhani, V. Petkov, C. F. Kisielowski, V. V. Volkov, Y. Zhu, G. Caruntu, A. P. Alivisatos, and R. Ramesh, *Nat. Mater.* **11**, 700 (2012).